Chemical state speciation by resonant Raman scattering

2002 J. Phys.: Condens. Matter 14 12367

(http://iopscience.iop.org/0953-8984/14/47/311)

INSTITUTE OF PHYSICS PUBLISHING JOURNAL OF PHYSICS: CONDENSED MATTER

J. Phys.: Condens. Matter **14** (2002) 12367–12381 PII: S0953-8984(02)33848-7

Chemical state speciation by resonant Raman scattering

A G Karydas[1,3], S Galanopoulos[1], Ch Zarkadas[1], T Paradellis[1,4] and N Kallithrakas-Kontos[2]

[1] Laboratory for Material Analysis, Institute of Nuclear Physics, NCSR 'Demokritos', Aghia Paraskevi, 153 10 Athens, Greece
[2] Technical University of Crete, Laboratory of Analytical and Environmental Chemistry, University Campus, 73100 Chania, Greece

E-mail: karydas@inp.demokritos.gr

Received 13 February 2002
Published 15 November 2002
Online at stacks.iop.org/JPhysCM/14/12367

Abstract

In the resonant Raman scattering (RRS) process the emitted photon exhibits a continuous energy distribution with a high energy cutoff limit. This cutoff energy depends on the chemical state of the element under examination. In the present work, the possibility of identifying the chemical state of V atoms by employing RRS spectroscopy with a semiconductor Si(Li) detector is investigated. A proton induced Cr Kα x-ray beam was used as the incident radiation, having a fixed energy lower than the V K-absorption edge. The net RRS distributions extracted from the energy dispersive spectra of metallic V and its compound targets were simulated by an appropriate theoretical model. The results showed the possibility of employing RRS spectroscopy with a semiconductor detector for chemical speciation studies.

1. Introduction

The determination of the oxidation state of an element in a compound constitutes a well motivated problem in x-ray analytical studies of environmental, biological and industrial materials [1–3]. Towards this aim efforts have been directed to the possibility of identifying the elements of a sample as well as their oxidation states by a single measurement in an energy dispersive detector system [4–6]. The chemical bonding of an element affects the emission of its characteristic x-rays in various ways. The formation of chemical bonding causes a migration of the valence electrons among participating atoms, thus reducing screening effects and increasing their inner shell binding energies [7]. This fact results in the chemical shifts of the energies of Kα, K$\beta_{1,3}$ and Kβ' emission lines from compound targets of an element

[3] Author to whom any correspondence should be addressed.
[4] Sadly, T Paradellis passed away on 24 March 2002.

with respect to the metallic state. Papp *et al* [4] have discussed the current potential of solid-state detectors to offer chemical state sensitivity in proton induced x-ray emission (PIXE) studies and how the advances in signal processing can help. In the same work it was reported that since the peak centroid can be determined with an accuracy better than 0.4 eV in the 3–20 keV energy region, shifts of the order of 1–2 eV usually appearing in the energy difference $K\beta - K\alpha$ can be measured for the matrix elements of the analysed samples. Shifts up to 2 eV have been measured by Kallithrakas-Konto [5] in the $K\beta - K\alpha$ energy differences of Cr and Mn compounds by the use of an energy dispersive detection system with a ^{109}Cd excitation source. The chemical environment, apart from the creation of chemical shifts, alters the relative intensities of K [6, 8] and L [9] characteristic x-ray lines, changes their natural width [8] and creates satellite lines, the so-called 'white lines' or 'exciton lines' [10, 11]. These lines are produced from transitions in orbitals, which are occupied in the neutral atom. Yasuda and Kakiyama [8] have measured the shifts which appear in the energies of $K\alpha_1$, $K\beta_{1,3}$ and $K\beta_5$ characteristic lines for different oxidation states of V with a two-crystal x-ray spectrometer. They also measured the changes in their relative intensities and presented a linear relationship between V $K\alpha_1$ width and V $K\alpha_1$/V $K\alpha_2$ intensity ratio.

The resonant Raman scattering (RRS) is an inelastic process which exhibits a strong resonant behaviour as the energy of the incident radiation approaches from lower energies an absorption edge of an element [12]. The resonant character of the process and the existence of an onset energy in the RRS spectrum enable the probing of the edge structure characteristics by simply tuning the incident radiation towards the edge [13]. High resolution RRS spectroscopy has been already investigated as a probe for chemical speciation and for examining the electronic, as well as the geometrical structure of materials [10, 11, 14, 15]. The characteristic feature of these experiments was the high resolution (1–2 eV or better) of the incident radiation and, also, of the scattered radiation detection. The scanning of the absorption edge by the incident beam causes progressive changes in the scattered spectra, and allows the study of the dependence of the maximum RRS energy with respect to the energy of the incident radiation and the oxidation state of the element. Udagawa and Tohji [14] acquired RRS spectra from metallic Cu, CuO and Cu_2O, before and across the resonant energy region, concluding that the detailed structure of each scattered spectrum reflects the differences in the electronic structure of the substances. The RRS spectra from metallic Cu and Cu_2O exhibited many similarities, in contrast to CuO.

Miyano *et al* [11] observed two peaks in the RRS emission spectra of K and Cl from the KCl compound, when the incident radiation varied, just below the corresponding K-shell absorption edges. These two structures were in full accordance with the corresponding features found in the K-shell absorption spectra of the two elements. Moreover, the energy offsets between the RRS emission data and theoretical predictions offered a qualitative explanation for the excitonic nature of the observed peaks.

The aim of the present work is the investigation of the possibility of chemical speciation determination using low resolution RRS spectroscopy. The incident radiation had a fixed energy difference from an inner-shell absorption edge of vanadium and the RRS spectrum was detected by a Si(Li) detector. A proton induced Cr $K\alpha$ x-ray beam with energy $E_0 = 5411.6$ eV [16] was employed in the measurement of RRS emission spectra from V, in its metallic state and in various compounds (VO_2, $NaVO_3$ and Na_3VO_4). The incident radiation which had a 53.5 eV lower energy than the V free atom K absorption edge $U_K = (5465.1 \pm 0.3)$ eV [17] gives rise to a strong contribution of the RRS process in the energy spectrum.

2. RRS energy distribution and chemical state effect

The interaction Hamiltonian between the electromagnetic field of an incident photon, expressed by the vector potential $\vec{A}$ and an atomic electron with momentum $\vec{p}$ includes the quadratric $\vec{A}\cdot\vec{A}$ term and the linear $\vec{A}\cdot\vec{p}$ one. Both terms can give contributions to a scattering process; the quadratic term describes the Rayleigh or Compton scattering in first order perturbation theory, whereas the $\vec{A}\cdot\vec{p}$ term the RRS taken in second order in order to preserve the number of photons. The Kramers–Heisenberg formula [13] is the theoretical basis for the calculation of the differential scattering cross-section by both contributions, which can be at the same order of magnitude under specific experimental conditions [18, 19]. When the energy E_0 of the incident radiation is just below an inner shell binding energy, the RRS proceeds via the creation of a whole set of intermediate states which include an electron in the continuum and a corresponding hole in the inner atomic shell. After integration over all possible electron emission energies, the KL-RRS ($E_0 \leqslant U_{\mathrm{K}}$) differential cross-section per unit scattered energy E_s and per unit solid angle can be written in the following form [13]:

$$\left(\frac{\mathrm{d}\sigma}{\mathrm{d}\Omega\,\mathrm{d}E_s}\right)_{\mathrm{KL}} = \frac{r_0^2}{2}\frac{E_s}{E_0}\frac{(U_{\mathrm{K}}+\overline{T_e})\cdot(U_{\mathrm{K}}-U_{\mathrm{L}})}{(U_{\mathrm{K}}-U_{\mathrm{L}}-E_s)^2+(\Gamma_{\mathrm{K}}/2)^2}g_{1\mathrm{s},2\mathrm{p}}\left(\frac{\mathrm{d}g_{\mathrm{K}}}{\mathrm{d}T_e}\right)_{U_{\mathrm{K}}+\overline{T_e}} \tag{1}$$

where r_0^2 is the electron radius squared (equal to 79.4 mb), U_{L} is the average $\mathrm{L}_{2,3}$ binding energy, $\overline{T_e}$ is the average electron kinetic energy in the continuum, Γ_{K} is the total K-shell width and $g_{1\mathrm{s},2\mathrm{p}}$ is the oscillator strength between the $(1\mathrm{s})^{-1}$ and $(2\mathrm{p})^{-1}$ hole states, whereas $\mathrm{d}g_{\mathrm{K}}/\mathrm{d}T_e$ represents the oscillator density which is proportional to the density of empty states in the continuum. The factors $g_{1\mathrm{s},2\mathrm{p}}$ and $\mathrm{d}g_{\mathrm{K}}/\mathrm{d}T_e$, are expressed as follows [20]:

$$\left(\frac{\mathrm{d}g_{\mathrm{K}}}{\mathrm{d}T_e}\right)_{U_{\mathrm{K}}+\overline{T_e}} = \frac{\tau_{\mathrm{K}}(U_{\mathrm{K}}+\overline{T_e})}{2\pi^2\hbar c r_0}, \qquad g_{1\mathrm{s},2\mathrm{p}} = \frac{1}{2}\frac{\Gamma_{\mathrm{K}\alpha}\hbar c}{r_0(U_{\mathrm{K}}-U_{\mathrm{L}})^2} \tag{2}$$

where $\Gamma_{\mathrm{K}\alpha}$ is the Kα line radiative width and $\tau_{\mathrm{K}}(U_{\mathrm{K}}+\overline{T_e})$ the K-shell photoelectric cross-section at the energy $U_{\mathrm{K}}+\overline{T_e}$. By combining the expressions (1) and (2), the KL-RRS differential cross-section per unit scattered energy E_s and solid angle is written in the following form:

$$\left(\frac{\mathrm{d}\sigma}{\mathrm{d}\Omega\,\mathrm{d}E_s}\right)_{\mathrm{KL}} = \frac{\Gamma_{\mathrm{K}\alpha}}{8\pi^2}\frac{(U_{\mathrm{K}}+\overline{T_e})\tau_{\mathrm{K}}(U_{\mathrm{K}}+\overline{T_e})}{(U_{\mathrm{K}}-U_{\mathrm{L}})E_0}\frac{E_s}{(U_{\mathrm{K}}-U_{\mathrm{L}}-E_s)^2+(\Gamma_{\mathrm{K}}/2)^2}. \tag{3}$$

From the above expression it can be observed that the profile of the RRS emission spectrum appears to be a Lorentzian distribution centred at the energy $(U_{\mathrm{K}}-U_{\mathrm{L}}) \equiv E_{\mathrm{K}\alpha}$. However, the energy conservation between the initial and final states of the process implies that the RRS spectrum should exhibit a cutoff energy E_s^m given by the following relationship:

$$E_s^m = E_0 - U_{\mathrm{L}}. \tag{4}$$

The energy E_s^m corresponds to the case of an emitted electron having zero kinetic energy. A schematic diagram, which describes qualitatively the characteristics of the RRS spectrum, is shown in figure 1. If the element participates in chemical bonding, the shift of its U_{L} binding energy to slightly higher energies will be directly reflected in a shift of the high energy RRS threshold to a lower energy. More specifically, if ΔE_b is the perturbation in the L-shell binding energy due to the chemical bonding, the maximum RRS energy from an atom bound in a molecule will be given by

$$E_s'^m = E_0 - (U_{\mathrm{L}} + \Delta E_b). \tag{5}$$

The shift to a lower maximum scattered energy will also result in a decrease in the total RRS intensity, since a slice from the RRS distribution with width equal to ΔE_b will be cut

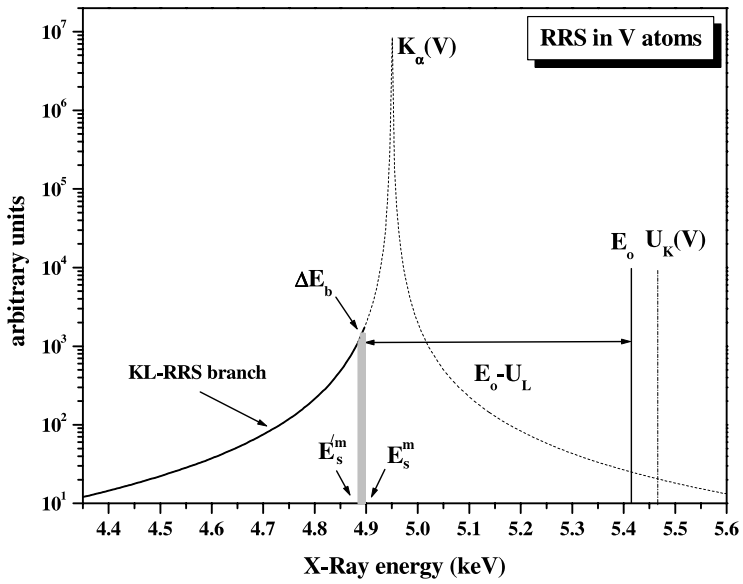

Figure 1. Schematic representation of the RRS emission spectrum and the effect of the chemical bonding.

(figure 1). The shifts that are expected to be observed in the RRS high energy threshold are significantly higher than those observed in the characteristic x-rays, and can vary up to 2 eV/oxidation state [10]. Bajt *et al* [21] studied Cr compounds by x-ray absorption near edge structure (XANES) spectroscopy and they found that the K edges of chromium in Cr_2O_3 and $(CrO_4)^{2-}$ were 7 and 15 eV greater than that of the metallic state.

3. Experimental details

A proton beam of energy 1.5 MeV was used for the production of the Cr K characteristic x-rays. A V filter of 34 mg cm^{-2} was placed between the primary Cr target and the scatterer position in order to absorb selectively the Cr Kβ x-rays. A Si(Li) detector with 194 eV energy resolution at 5.9 keV was used for the detection of the RRS spectra. More details of the experimental set-up are given elsewhere [22]. The detector was calibrated for its energy–channel response, as well as for the dependence of the FWHM on the energy of the detected radiation by using the following expressions:

$$E = a\ \text{chan} + b \qquad \text{FWHM}^2 = c_2 E + c_1. \tag{6}$$

The results of the linear regression analysis for the parameters a, b, c_1 and c_2 are reported below:

$$\begin{aligned} a &= (4.490 \pm 0.003)\ \text{eV/chan} \qquad & b &= (-42.3 \pm 2.5)\ \text{eV} \\ c_1 &= (28.22 \pm 0.75) \times 10^{-3}\ \text{keV}^2 \qquad & c_2 &= (1.59 \pm 0.23) \times 10^{-3}\ \text{keV}. \end{aligned} \tag{7}$$

The energy stability of the spectrometer was examined for a period of one week by irradiating a thin Ti target; it was found to be better than 1 eV/24 h for the peak centroid and 1.5 eV/24 h for the FWHM. Targets of metallic vanadium, VO_2, $NaVO_3$ and Na_3VO_4, were prepared in the form of pellets after grinding and pressing of fine powder material under a pressure of about 6 ton. The water content was measured by drying the powder material in an oven at 105 °C over 24 h. For all the compounds the water content was found to be less than

1%. The vanadium targets were irradiated in a Mo tube—yttrium secondary target assembly and the measured V Kα peak intensities were finally expressed in cps(mA (μg cm^{-2}))$^{-1}$. In these units, the V Kα peak intensities obtained from the V-compound pellets were found to vary down to 92% of the corresponding V-metal foil intensity. This can be probably attributed either to the variations of the packing ratios for each pellet, or to the existence of grains, causing particle size effects. By comparing the compound V Kα intensities with respect to that of the metal foil, appropriate correction factors were obtained for each pellet and applied next to the corresponding RRS yield.

The incident and the scattered radiation form angles of 45° with the scatterer surface. The number $Y_{RRS}(i)$ of RRS photons which are detected at a channel i which corresponds to a mean energy E_i is expressed via the following relationship [22]:

$$Y_{RRS}(i) = I_0 \Delta\Omega_d \left[\int_{E_i - \frac{a}{2}}^{E_i + \frac{a}{2}} \left(\frac{\mathrm{d}\sigma}{\mathrm{d}\Omega \, \mathrm{d}E'_s} \right)_{RRS} \mathrm{d}E'_s \right] \frac{N_{AV}}{A_w} \frac{Q c_{pur} f_{cor} f_{abs}(E_i) \varepsilon_d(E_i)}{\mu_s(E_0) + \mu_s(E_i)} \tag{8}$$

where I_0 is the number of incident photons per μC that irradiate the scatterer, $\Delta\Omega_d$ is the detector solid angle, the differential RRS cross-section is given by equation (3) in r_0^2/(sr keV) units, a is the slope of the energy–channel relationship, N_{AV} is the Avogadro number, A_w is the atomic weight of vanadium, $\mu_s(E_0)$ and $\mu_s(E_i)$ are the mass absorption coefficients of the incident and scattered radiation respectively expressed in cm^2 g^{-1}, Q is the total accumulated charge, $f_{abs}(E_i)$ is the absorption correction factor for the scattered x-rays in the very thin organic materials used for sample support and for maintaining the vacuum inside the irradiation chamber, $\varepsilon_d(E_i)$ is the detector efficiency at energy E_i, c_{pur} is the concentration of vanadium in the analysed compound and f_{cor} is the correction factor for packing ratio/particle size effects. Prior to any measurement of the RRS cross sections the calibration factor $I_0\Delta\Omega_d$ has to be evaluated. Pure spectroscopic targets with $Z = 14$–20 were analysed and their characteristic Kα x-ray intensities, with the theoretical fluorescence cross-sections were employed in the evaluation of the $I_0\Delta\Omega_d$ factor, which was found to be equal to $(10.0 \pm 0.8) \times 10^4$ (counts μC^{-1}) sr. For the calculation of the detector efficiency the nominal layer thickness of the Be window, Au contact layer and Si dead layer were used.

4. Fitting of the RRS spectrum

A typical RRS spectrum obtained using a vanadium foil as a scatterer is shown in figure 2. The spectrum includes an intense total Rayleigh and Compton V Kα scattered peak at the high energy part and an RRS distribution asymmetric to the lower energies. The various scattered peaks are located on the continuous γ-ray induced background, which extends to zero energy and exhibits a smooth behaviour in the energy spectrum. All the vanadium spectra were acquired to the same RRS peak intensity in order to have similar statistical uncertainties, whereas a background spectrum was obtained by irradiating the sample holder alone. After every vanadium compound measurement, the V foil was also measured under the same experimental conditions in order to compare the corresponding spectra.

Before any description of the RRS spectrum, the total scattered Rayleigh (R) and Compton V Kα peak has to be simulated. Although for the elastic peak a Gaussian distribution would be adequate, the Compton scattered peak exhibits an asymmetric distribution to the lower energies and its tail interferes with the beginning of the RRS distribution. Moreover, due to the infinite thickness of the scatterers used, double-Compton-scattering events are expected to appear in the spectrum. The approach that was adopted for the description of the R and C V Kα peaks in the RRS spectra was based on the introduction of two reference spectra, which, after a linear superimposition, can describe the energy response of the two peaks in

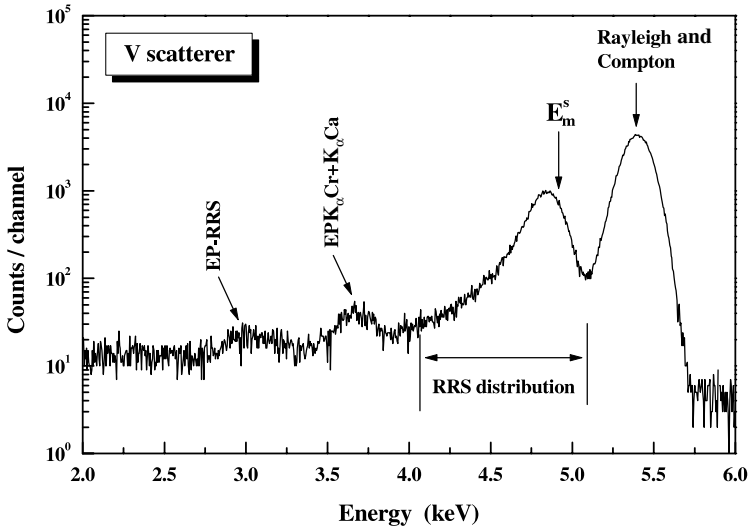

Figure 2. Characteristic components of a typical energy dispersive RRS emission spectrum.

Table 1. Theoretical scattering (Rayleigh, Compton) cross-sections for the incident radiation in Kapton and metallic Fe. In the last two columns, the corresponding measured and theoretical predicted scattered yields of the incident radiation are presented.

Scatterer	$(\mathrm{d}\sigma/\mathrm{d}\Omega)_{Compton}$ (cm^2 g^{-1})	$(\mathrm{d}\sigma/\mathrm{d}\Omega)_{Rayleigh}$ (cm^2 g^{-1})	I_{exp} (counts μC^{-1})	I_{theo} (counts μC^{-1})
Kapton	7.6×10^{-3}	11.5×10^{-3}	27.2 ± 0.5	27.5 ± 2.8
Fe	3.7×10^{-3}	0.115	31.0 ± 0.6	46.2 ± 4.6

the whole spectrum. As a guideline, R and C scattering cross-sections [23] were employed for an estimation of the theoretical total scattered yield. Experimentally, an organic material (Kapton) having a thickness of 17 mg cm^{-2} and a thick iron target were used. In the case of Kapton the experimental yield was found in very good agreement with the theoretically calculated value (table 1). The experimental scattered yield from Fe was found to be 30% less than that expected (table 1), but this can be explained due to the polycrystalline nature of the Fe metal, which in certain directions can reduce the expected intensity of Rayleigh scattering [24]. However, even in this case the R component is estimated to account for 96% of the total measured scattered intensity. The Fe and Kapton scattered spectra, after subtraction of the γ-ray induced background component, are shown in figure 3. By use of the reference spectra of figure 3, the energy response of the total R plus C scattered peak in any RRS spectrum can be described as follows:

$$Y_{RC}(i) = a_R Y_R^{\mathrm{Fe}}(i) + a_C Y_{RC}^{kapt}(i) \tag{9}$$

where $Y_R^{\mathrm{Fe}}(i)$and $Y_{RC}^{kapt}(i)$ express the counts per channel i which have been recorded in the scattered spectra of Fe and Kapton materials respectively, and a_R, a_C are fitting parameters.

Assuming an isotropic emission, the differential RRS energy distribution (equation (3)) can be expressed as

$$\left(\frac{\mathrm{d}\sigma}{\mathrm{d}\Omega\,\mathrm{d}E_s}\right)_{\mathrm{KL-RRS}} = C(E_0)\frac{1}{4\pi}\frac{E_s}{(U_{\mathrm{K}} - U_{\mathrm{L}} - E_s)^2 + (\Gamma_{\mathrm{K}}/2)^2} \tag{10}$$

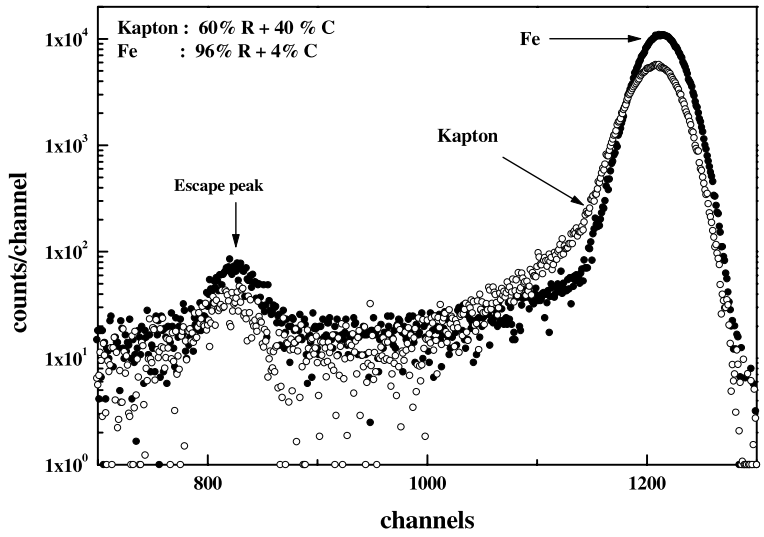

Figure 3. Reference scattered spectra for the incident radiation from Kapton and metallic Fe.

where $C(E_0)$ is a proportionality factor expressed in r_0^2 units. For the V atom, $U_{\mathrm{K}} = (5465.1 \pm 0.3)$ eV [16], $U_{\mathrm{L}} = (515.4 \pm 0.3)$ eV [16] and $\Gamma_{\mathrm{K}} = \Gamma_{\mathrm{K}\alpha}/\omega_{\mathrm{K}} = 1.065$ eV, where $\Gamma_{\mathrm{K}\alpha}$ and ω_{K} were obtained from [24] and [25] respectively. The number of total detected counts in any arbitrary channel i of the RRS spectrum is obtained after the summation of all partial contributions, namely the R and C scattered peaks, the RRS distribution and possibly the characteristic peaks produced by trace elements contained in the scatterer matrix:

$$Y_{tot}(i) = Y_{RRS}^{convo}(i) + Y_{RC}(i) + \mathrm{peak}(i,k) \tag{11}$$

where

$$Y_{RRS}^{convo}(i) = \sum_{j=\mathrm{chan}(E_{s,min})}^{\mathrm{chan}(E_s'^m)} \mathrm{gauss}[i, j, hg_N(j), \sigma(j)] \cdot Y_{RRS}(j) \tag{11a}$$

$$\mathrm{peak}(i,k) = \mathrm{gauss}[i, k, hg(k), \sigma(k)]. \tag{11b}$$

The term $Y_{RRS}^{convo}(i)$ expresses the convoluted RRS distribution and includes a summation over all the channels over which the RRS structure is extended, while the $Y_{RRS}(j)$ is the theoretical RRS yield at channel j calculated by equation (8). The function $\mathrm{chan}(E_i)$ is the inverse relationship of the energy–channel formula (equation (6)), whereas $E_{s,min}$ is the lower energy threshold of the RRS distribution. The high energy onset $E_s'^m$ is given by equation (5) as a function of the perturbation energy ΔE_b. The function $\mathrm{gauss}[i, j, hg_N(j), \sigma(j)]$ denotes a Gaussian distribution normalized to unit area having as centroid the channel j, standard deviation $\sigma(j) = 0.4247\,\mathrm{FWHM}(j)$ and height at the centroid channel equal to $hg_N(j)$ expressed as follows:

$$hg_N(j) = \frac{1}{\sqrt{2\pi}\sigma(j)}. \tag{12}$$

The term $\mathrm{peak}(i,k)$ expresses the contribution at the channel i of a low intensity peak having a centroid at channel k. Therefore the RRS energy spectrum can be described by the use of a non-linear fitting procedure applied in equation (11). For the RRS distribution the parameters

$C(E_0)$ and ΔE_b have to be fitted, whereas the energy response of the total scattered peak introduces the parameters a_R and a_C. Furthermore, the energy–channel and FWHM–energy relationships include the α, b, c_1, c_2 parameters with central values and standard deviations given by equation (7).

In order to fit the RRS spectra the non-linear least squares program MINUIT was employed [27]. The calculation of the RRS intensity per channel, $Y_{RRS}(i)$, was performed by Simpson integration of the cross-section given by equation (10). The fitting procedure was performed in two steps. In the first step, the whole RRS spectrum was fitted and the parameters α, b, c_1, c_2 were allowed to vary inside one sigma interval. For all the other fitted parameters no restriction was applied. Results are presented in figures 4(a) and (b), for vanadium and $NaVO_3$ RRS spectra; the partial contributions are also indicated. The obtained X^2 values were less than three for all the fitted spectra. In the second step, the fitted R, C scattered and any other characteristic peaks were subtracted from the experimental spectra to obtain the net RRS distributions. The high energy parts of the obtained net RRS distributions are presented in figure 5 normalized to their corresponding maxima for comparison reasons. For V metal and the VO_2 compound the labels (a, b, c) correspond to net RRS distributions obtained at different times. From this figure it can be observed that there is a shift of two to three channels to lower energies for the spectra obtained from V compounds relative to that of the V foil. This displacement should appear if the RRS high energy onset has been shifted to lower energies in the case of V compounds. The net RRS contributions of each compound were again fitted using equation (11*a*). This time the parameters α, b, c_1 and c_2 were fixed at their initial central values and the parameters $C(E_0)$ and ΔE_b were found for each RRS distribution. All the obtained X^2 values were less than two and the obtained fitted RRS distributions for the V metal and $NaVO_3$ compound are presented in figures 6(a) and (b).

5. Results and discussion

From the fitting procedure of the net RRS distributions the parameters $C(E_0)$ and ΔE_b were determined (table 2). Since we are interested in the chemical shift differences between compounds and metallic V, the values $\Delta E_b^* = \Delta E_b(\text{comp}) - \Delta E_b(\text{metal})$ are reported in the last column of table 2, with associated errors calculated by error propagation. The final chemical shift values indicate a trend to increase with the increment of the V oxidation number state, but the reported values are quoted with rather high uncertainties. Thus, a different approach was also applied for the determination of the chemical shifts. The net RRS distributions (figures 6(a) and (b)) can be fitted in a restricted interval of $\pm 1\sigma$ around the centroid channel by simply employing a Gaussian distribution. Therefore, if two net RRS distributions $g_1(i)$ and $g_2(i)$ are normalized to the same maximum centroid intensity and the corresponding counts per channel are next subtracted in a logarithmic scale [4], the following linear relationship is obtained:

$$\Delta(\ln G) \equiv \ln(g_1(i)) - \ln(g_2(i)) = \frac{\alpha \Delta E_b^{**}}{\sigma^2} i + b' \tag{13}$$

where ΔE_b^{**} is the shift (in eV) of the two Gaussian centroids, α is the slope of the energy–channel relationship expressed in eV/channel and σ denotes an average standard deviation of all Gaussians, found to be equal to (82 ± 7) eV. It is important to note here that the shift between the two Gaussian centroids will be equal to the corresponding shift in the $E_s'^m$ values of the theoretical RRS distributions. In order to test this argument, theoretical RRS distributions were generated, with or without a given upper energy shift, and then convoluted with a Gaussian function. After several comparisons it was confirmed that the shifts found via

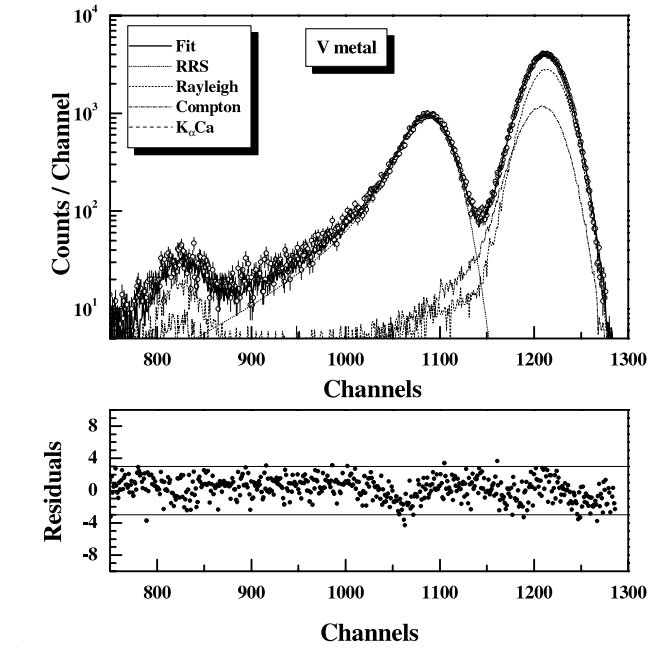

(b)

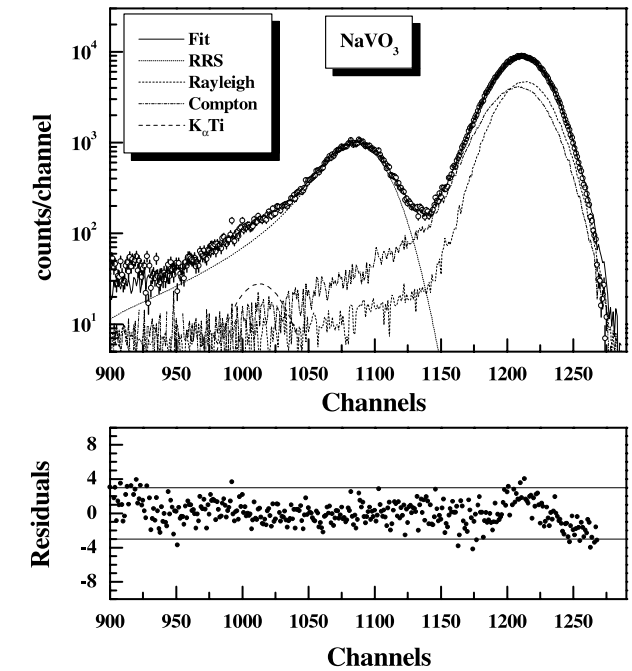

Figure 4. (a) Non-linear least squares fitting of the metallic V RRS spectrum and the corresponding residuals. (b) Non-linear least squares fitting of the $NaVO_3$ compound RRS spectrum and the corresponding residuals.

equation (13) were equal to the one artificially introduced in the onset energy of the theoretical RRS distributions.

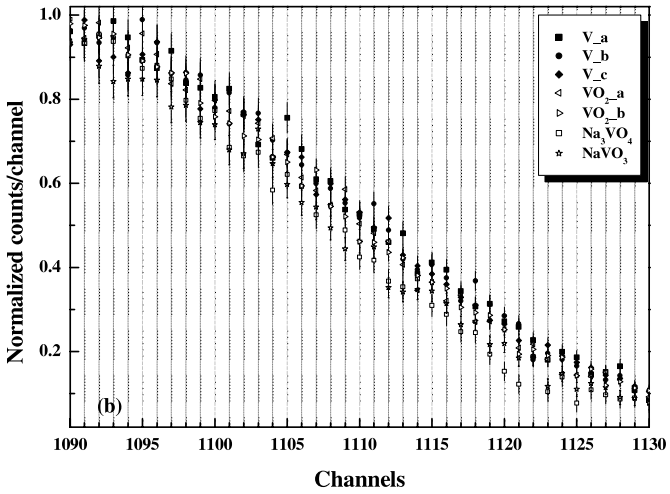

Figure 5. High energy part of the net RRS distributions of metallic V and its compounds, obtained after subtraction from the experimental spectra of all the other fitted spectrum components. Spectra acquired at different times are labelled as a, b and c respectively.

Table 2. Results for the proportionality factor $C(E_0)$ of the RRS cross-section (equation (10)) and for the chemical shift ΔE_b (equation (5)), after the application of the MINUIT fitting procedure in the net RRS distributions. The ΔE_b^* values represent the chemical shifts observed in V atoms with different oxidation states relative to the metallic case.

V compound	Oxidation state	$C(E_0)$ (r_0^2)	ΔE_b (eV)	ΔE_b^* (eV)
V metallic	0	4.4 ± 0.4	5.9 ± 3.8	0
VO_2	+4	4.6 ± 0.4	12.3 ± 3.4	6.4 ± 5.0
$NaVO_3$	+5	4.4 ± 0.4	14.0 ± 4.0	8.1 ± 5.5
Na_3VO_4	+5	4.5 ± 0.5	16.9 ± 4.1	11 ± 5.5

Since metallic V and VO_2 RRS spectra were acquired in triplicate and duplicate respectively, we have plotted in figure 7 as a function of the channel number the $\Delta(\ln G)$ differences between spectra obtained from the same scatterer material, but acquired at different times. The results of the linear fitting are reported in table 3, together with the corresponding chemical shifts ΔE_b^{**}. No chemical shift significantly different than zero was observed for these cases. However, by comparing the net RRS spectra between metallic V and the corresponding one from the various V compounds, we obtain the $\Delta(\ln G)$ dependence shown in figure 8. After linear fitting, the chemical shifts, reported also in table 3 were obtained. The final uncertainties included in the ΔE_b^{**} values are considerably lower than that found in the previous procedure (ΔE_b^* shifts), but both shifts are in good agreement. In the last column of table 3 calculated photoelectron $2p^{3/2}$ chemical shifts are shown from [27] and are in rather good agreement with our experimental ΔE_b^{**} values.

Using the $C(E_0)$ and ΔE_b^* values, experimental total RRS cross-sections can be calculated by integrating equation (10), as follows:

$$\left(\frac{\mathrm{d}\sigma}{\mathrm{d}\Omega}\right)_{RRS} = C(E_0)\frac{1}{4\pi}\int_{E_{s,min}}^{E_s^m} \mathrm{d}E_s' \frac{E_s'}{(U_\mathrm{K} - U_\mathrm{L} - E_s')^2 + (\Gamma_\mathrm{K}/2)^2}. \tag{14}$$

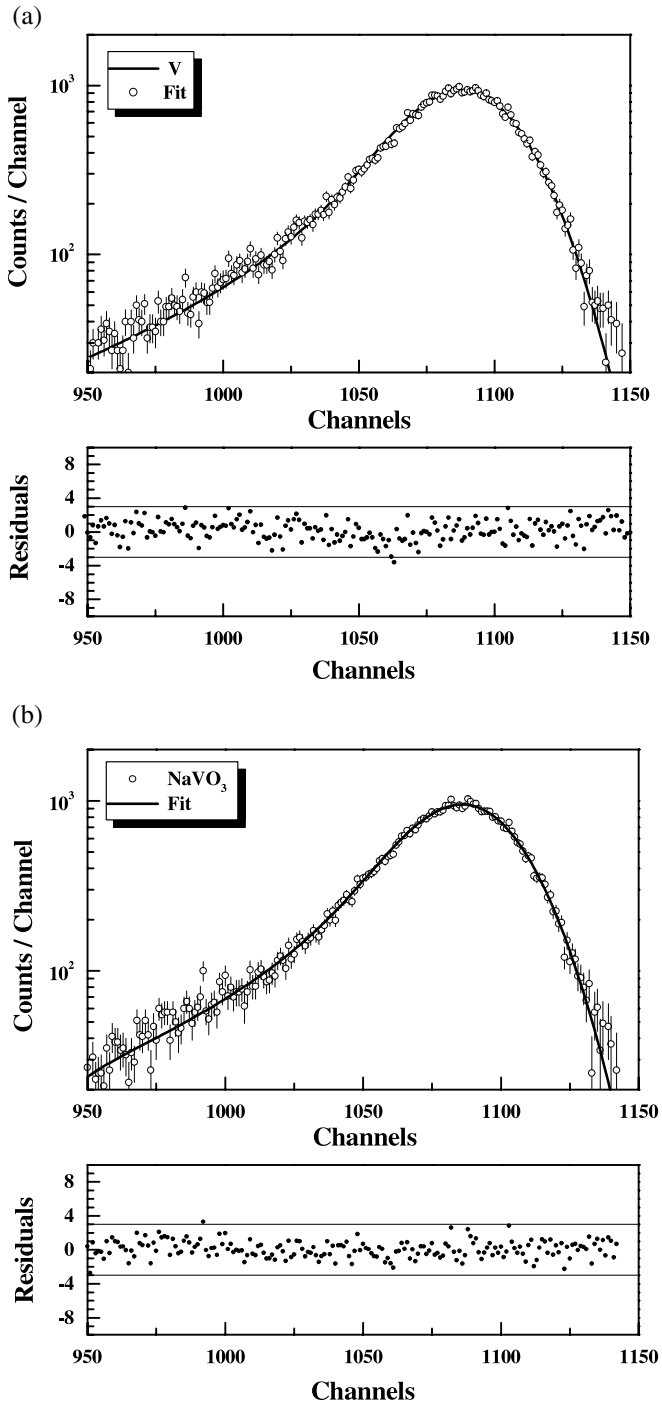

Figure 6. (a) Non-linear least squares fitting of the net RRS distribution obtained from the metallic V. (b) Non-linear least squares fitting of the net RRS distribution obtained from the $NaVO_3$ compound.

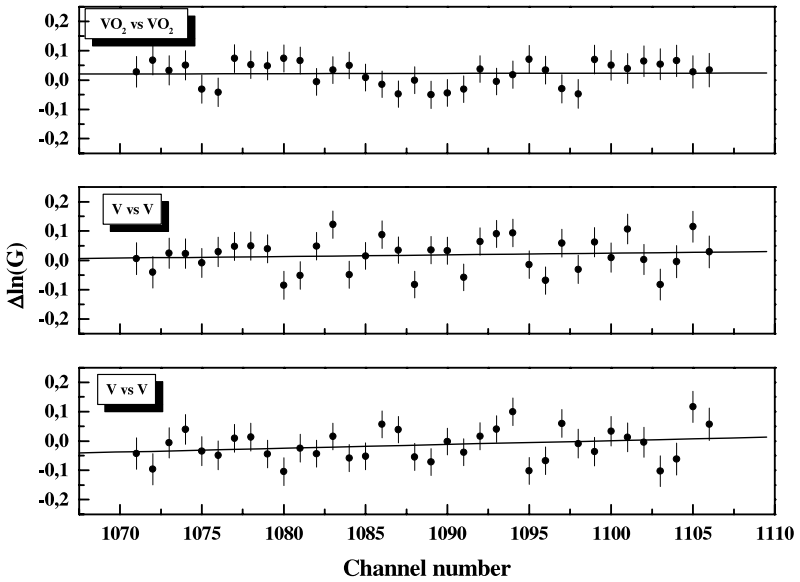

Figure 7. Dependence of the parameter $\Delta(\ln G)$ (equation (13)) with the channel number in the region of 1σ around the Gaussian centroid, calculated between the net RRS distributions obtained from different spectra of the same target.

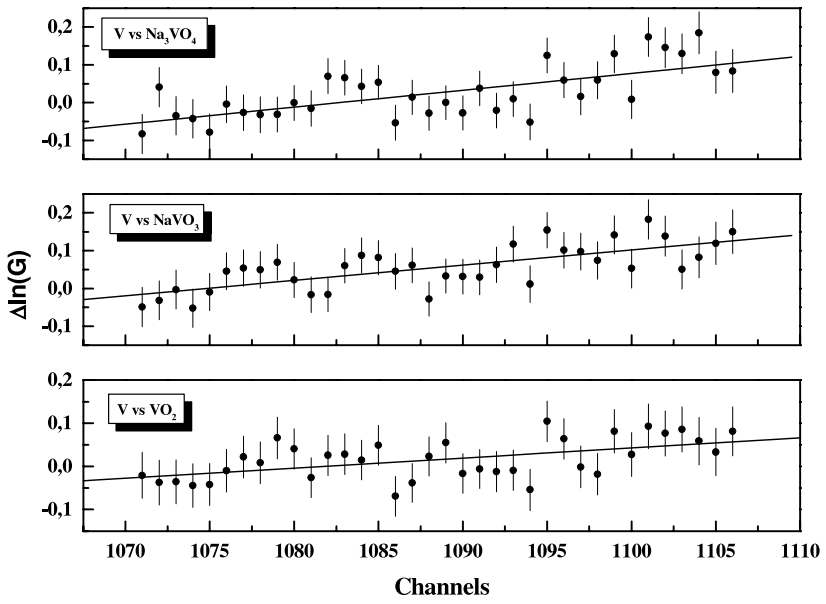

Figure 8. Dependence of the parameter $\Delta(\ln G)$ (equation (13)) with the channel number in the region of 1σ around the Gaussian centroid, calculated between the net RRS distributions from targets with different oxidation states of V.

As a lower energy integration limit the energy 4220 eV was used which results in lower cross-section (about 3.5%), relative to that obtained by integrating from zero energy. The upper energy RRS threshold was obtained by equation (5) using the ΔE_b^* values of table 2. The results are presented in table 4. The total RRS cross-section can also be calculated by summing all

Table 3. The chemical shifts obtained via equation (13) by comparing the net RRS distributions between metallic V and its compounds (ΔE_b^{**} values), are presented together with the corresponding one extracted from the MINUIT fitting procedure (ΔE_b^{*} values). In the last column, the energy shifts, which have been calculated for the $2p^{3/2}$ photoelectron emission line of the corresponding V compounds are presented from [28].

Spectra comparison	Slope (channel^{-1})	ΔE_b^{**} (eV)	ΔE_b^{*} (eV)	CS–$2p^{3/2}$ [28] (eV)
V versus V	$(1.3 \pm 0.9) \times 10^{-3}$	2.0 ± 1.3	—	—
V versus V	$(0.6 \pm 0.9) \times 10^{-3}$	0.8 ± 1.3	—	—
VO_2 versus VO_2	$(0.1 \pm 0.7) \times 10^{-3}$	0.1 ± 1.0	—	—
V versus VO_2	$(2.7 \pm 0.7) \times 10^{-3}$	4.1 ± 1.0	6.4 ± 5.0	4.1
V versus $NaVO_3$	$(4.3 \pm 0.9) \times 10^{-3}$	6.4 ± 1.2	8.1 ± 5.5	4.8
V versus Na_3VO_4	$(4.5 \pm 0.8) \times 10^{-3}$	6.8 ± 1.3	11 ± 5.5	5.1

Table 4. Experimental RRS cross-sections, obtained either after integration of formula (10) using for $C(E_0)$ and ΔE_b^{*} (included in the upper integration limit of (10)) the fitted values of table 2 (second column) or after summation of all the net RRS counts (third column). The theoretical cross-sections were calculated according to equations (3) and (5), using the measured ΔE_b^{**} chemical shifts.

V compound	$\left(\frac{d\sigma}{d\Omega}\right)_{RRS}$ (r_0^2 sr^{-1})	$\left(\frac{d\sigma}{d\Omega}\right)_{RRS}^{sum}$ (r_0^2 sr^{-1})	$\left(\frac{d\sigma}{d\Omega}\right)_{RRS}^{theo}$ (r_0^2 sr^{-1})
V metallic	28.8 ± 3.5	26.0 ± 2.6	23.5
VO_2	25.4 ± 3.1	24.0 ± 2.5	21.7
$NaVO_3$	23.5 ± 2.8	21.7 ± 2.3	20.8
Na_3VO_4	23.4 ± 2.8	21.5 ± 2.3	20.5

the events from the net RRS distributions and using an average outgoing scattered energy as follows:

$$\bar{E}_{RRS} = \mathrm{en}\left(\frac{\sum Y_{RRS}(i) \cdot i}{\sum Y_{RRS}(i)}\right). \tag{15}$$

The obtained experimental total RRS cross-sections denoted as $\left(\frac{d\sigma}{d\Omega}\right)_{RRS}^{sum}$, as well as the theoretical ones $\left(\frac{d\sigma}{d\Omega}\right)_{RRS}^{theo}$ calculated by the application of equation (3), are presented in table 4. The measured RRS cross section for the metallic V is in good agreement with the value reported previously by Karydas and Paradellis [22], equal to $(22.9 \pm 2.3)\ r_0^2\ \mathrm{sr}^{-1}$. It is interesting to normalize the experimental and theoretical RRS cross-sections, with respect to the corresponding one for metallic V (table 5). A good agreement between experimental and theoretical normalized values exists, and it is evident that an increment of the oxidation state of V results in a decrease in the total RRS cross-section, almost 2–3%/oxidation state. It should be noted here that the errors quoted with the experimental normalized cross-sections are less than that reported in the absolute values, due to the elimination of the calibration factor $I_0 \Delta\Omega_d$ and its associated error. In order to examine the 'sensitivity' of the RRS process to identify the chemical shift by measuring the RRS yield for a V compound relative to a metallic target, theoretical KL-RRS cross-sections were calculated as a function of the chemical shift (up to 8 eV) for various incident x-ray radiations with energies 10–100 eV lower than the V free atom K-shell energy. From figure 9 it can be observed that the normalized cross-sections show an appreciable variation with the increase of chemical shift, which becomes significantly higher as the incident radiation approaches the absorption edge.

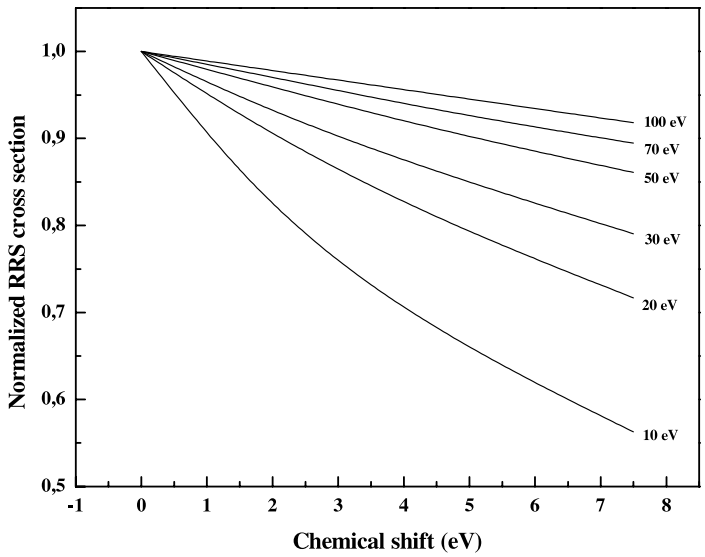

Figure 9. Dependence of the V KL-RRS cross-sections with the increase of the chemical shift, as a function of various incident x-ray radiations with energies 10–100 eV lower than the V K-shell energy.

Table 5. Comparison between theoretical and experimental RRS cross-sections of V at different oxidation states, normalized to the corresponding one of metallic V.

V compound	Experimental normalized RRS cross-sections	Theoretical normalized RRS cross-sections
V metal	1.0	1.0
VO_2	0.92 ± 0.04	0.94
$NaVO_3$	0.84 ± 0.04	0.88
Na_3VO_4	0.83 ± 0.04	0.87

6. Conclusions

The chemical state speciation of V compounds was investigated without using a tunable x-ray source, but taking advantage of the resonant Raman emission spectrum characteristics. An incident radiation having a fixed energy below the K absorption edge of V was used for the irradiation of various V compounds and a semiconductor Si(Li) detector recorded the scattered radiation. The comparison of the RRS emission spectra revealed a clear relationship: namely, increasing the oxidation state of V, its average $L_{2,3}$ binding energy is increased. The experimental results confirmed the theoretical estimations that the RRS vanadium cross-sections decrease as the oxidation state increases. The low resolution RRS spectroscopy can be considered as a competitive technique compared to other energy dispersive techniques that measure shifts of the characteristic x-ray lines. Although the RRS cross-sections are much lower than the fluorescence ones, the observed chemical shifts depend directly on the binding energy of an inner shell electron. Therefore, it is expected that they would be significantly higher than the shifts observed in the characteristic emission lines, since the latter depends on energy differences between two inner shell binding energies.

Acknowledgments

This work was supported by the General Secretary of Research and Technology, Ministry of Development, Greece, through the Greek–Slovenia bilateral project (EPAN-M.4.3, 2013555). We would like also to thank Drs M Kavčič and M Kobal from J Stefan Institute, Lujbljana for useful discussions and suggestions.

References

[1] Birks L S and Gilfrich J V 1978 *Spectrochim. Acta* B **33** 305–10
[2] Maeda K, Hasegawa K, Hamanaka H and Maeda M 1998 *Nucl. Instrum. Methods* B **136–138** 994–9
[3] Uda M, Yamamoto T and Tatebayashi T 1998 *Nucl. Instrum. Methods* B **150** 55–9
[4] Papp T, Campbell J L and Papp-Szabo E 2002 *Nucl. Instrum. Methods* B **189** 33–8
[5] Kallithrakas-Kontos N 1996 *Spectrochim. Acta* B **51** 1655–9
[6] Folkmann F 1996 *Nucl. Instrum. Methods* B **109/110** 39–41
[7] Hansen P G, Johnson B, Borchert G L and Schult O W B *Atomic Inner Shell Physics* ed B Crasemann (New York: Plenum) ch 6 pp 237–81
[8] Yasuda S and Kakiyama Y 1978 *X-Ray Spectrom.* **7** 23–5
[9] Sawhney K J S, Lodha G S, Kataria S K and Kulshreshtha S K 2000 *X-Ray Spectrom.* **29** 173–7
[10] Hanson A L, Bajt S, Johnsson B M, Meron M and Rivers M L 1993 *Phys. Lett.* **184** 143–7
[11] Miyano K E, Ma Y, Southworth S W, Cowan P L and Karlin B A 1996 *Phys. Rev.* B **54** 12022–8
[12] Sparks C J Jr 1974 *Phys. Rev. Lett.* **33** 262–5
[13] Manninen S 1997 *Radiat. Phys. Chem.* **50** 77–89
[14] Udagawa Y and Tohji K 1988 *Chem. Phys. Lett.* **148** 101–6
[15] Ma Y, Miyano K E, Cowan P L, Aglitzkiy Y and Karlin B A 1995 *Phys. Rev. Lett.* **74** 478–81
[16] Bearden J A and Burr A F 1967 *Rev. Mod. Phys.* **39** 125–42
[17] Bearden J A 1967 *Rev. Mod. Phys.* **39** 78–124
[18] Alexandropoulos N G and Cooper M J 1992 *International Tables for Crystallography* vol C, ed A J C Wilson pp 574–8
[19] Karydas A G, Budnar M, Šmit Ž, Zarkadas Ch and Paradellis T 2002 *Nucl. Instrum. Methods* B **189** 43–8
[20] Suortti P 1979 *Phys. Status Solidi* b **91** 657–66
[21] Bajt S, Clark S B, Sutton S R, Rivers M L and Smith J V 1993 *Anal. Chem.* **65** 1800
[22] Karydas A G and Paradellis T 1997 *J. Phys. B: At. Mol. Opt. Phys.* **30** 1893–905
[23] Hubbell J H, Veigele W J, Briggs E A, Brown R T, Cromer D T and Howerton R J 1975 *J. Phys. Chem. Ref. Data* **4** 471–511
[24] Karydas A G, Potiriadis C and Paradellis Th 1993 *X-Ray Spectrom.* **22** 387–94
[25] Scofield J H 1974 *At. Data Nucl. Data Tables* **14** 121–36
[26] Krause M O 1979 *J. Phys. Chem. Ref. Data* **8** 307–25
[27] MINUIT, Minimization Package, Reference Manual, Version 94.1, CERN Program Library Long Writeup D506
[28] Version 3.0 of the NIST XPS Database can be accessed online and free through the following internet address: http://srdata.nist.gov/xps/